HHS Public Access

Author manuscript

Neuroimage. Author manuscript; available in PMC 2019 August 01.

Published in final edited form as:

Neuroimage. 2018 August 01; 176: 489–498. doi:10.1016/j.neuroimage.2018.05.005.

Default Mode Network Abnormalities in Posttraumatic Stress Disorder: A Novel Network-Restricted Topology Approach

Teddy J. Akiki, M.D.[1,2], **Christopher L. Averill, B.S.**[1,2], **Kristen M. Wrocklage, Ph.D.**[1,2,3], **J. Cobb Scott, Ph.D.**[4,5], **Lynnette A. Averill, Ph.D.**[1,2], **Brian Schweinsburg, Ph.D.**[1,2], **Aaron Alexander-Bloch, M.D., Ph.D.**[2], **Brenda Martini, M.A.**[1,2], **Steven M. Southwick, M.D.**[1,2], **John H. Krystal, M.D.**[1,2], and **Chadi G. Abdallah, M.D.**[1,2]

[1]National Center for PTSD – Clinical Neurosciences Division, US Department of Veterans Affairs, West Haven, Connecticut

[2]Department of Psychiatry, Yale University School of Medicine, New Haven, Connecticut

[3]Gaylord Specialty Healthcare, Department of Psychology, Wallingford, Connecticut

[4]Department of Psychiatry, Perelman School of Medicine, University of Pennsylvania, Philadelphia, Pennsylvania

[5]VISN4 Mental Illness Research, Education, and Clinical Center at the Philadelphia VA Medical Center, Philadelphia, Pennsylvania

Abstract

Disruption in the default mode network (DMN) has been implicated in numerous neuropsychiatric disorders, including posttraumatic stress disorder (PTSD). However, studies have largely been limited to seed-based methods and involved inconsistent definitions of the DMN. Recent advances in neuroimaging and graph theory now permit the systematic exploration of intrinsic brain networks. In this study, we used resting-state functional magnetic resonance imaging (fMRI), diffusion MRI, and graph theoretical analyses to systematically examine the DMN connectivity and its relationship with PTSD symptom severity in a cohort of 65 combat-exposed US Veterans. We employed metrics that index overall connectivity strength, network integration (global efficiency), and network segregation (clustering coefficient). Then, we conducted a modularity and network-based statistical analysis to identify DMN regions of particular importance in PTSD. Finally, structural connectivity analyses were used to probe whether white matter abnormalities are associated with the identified functional DMN changes. We found decreased DMN functional connectivity strength to be associated with increased PTSD symptom severity. Further topological characterization suggests decreased functional integration and increased segregation in subjects

Corresponding Author: Chadi G. Abdallah, M.D.; Clinical Neurosciences Division – VA National Center for PTSD; Department of Psychiatry, Yale University School of Medicine; 950 Campbell Avenue, 151E West Haven, Connecticut 06516; Tel: 347-987-0717; Fax: 203-937-3481; chadi.abdallah@yale.edu.

Disclosure

All other authors report no competing interests.

with severe PTSD. Modularity analysis suggest a spared connectivity in the posterior DMN community (posterior cingulate, precuneus, angular gyrus) despite overall DMN weakened connections with increasing PTSD severity. Edge-wise network-based statistical analyses revealed a prefrontal dysconnectivity. Analysis of the diffusion networks revealed no alterations in overall strength or prefrontal structural connectivity. DMN abnormalities in patients with severe PTSD symptoms are characterized by decreased overall interconnections. On a finer scale, we found a pattern of prefrontal dysconnectivity, but increased cohesiveness in the posterior DMN community and relative sparing of connectivity in this region. The DMN measures established in this study may serve as a biomarker of disease severity and could have potential utility in developing circuit-based therapeutics.

Keywords

functional MRI; diffusion MRI; intrinsic connectivity networks; graph theory; PTSD; Veterans

1. Introduction

Intrinsic connectivity networks (ICNs)—networks of functionally coupled regions with high spatial consistency—have been identified as organizational elements of the human brain (Damoiseaux et al., 2006; Laird et al., 2011). One of the most consistently identifiable ICN is known as the default mode network (DMN), comprising aspects of the ventromedial prefrontal cortex (vmPFC), dorsomedial PFC (dmPFC), posterior cingulate cortex (PCC), precuneus, medial temporal lobe, and medial and lateral parietal cortices (Andrews-Hanna et al., 2010; Buckner et al., 2008; Yeo et al., 2011).

Several groups have seeded known structures of the DMN (e.g., PCC) and found evidence of alterations in DMN functional connectivity in PTSD (Bluhm et al., 2009; Daniels et al., 2011; DiGangi et al., 2016; Lanius et al., 2010; Miller et al., 2017a; Miller et al., 2017b; Qin et al., 2012; Shin et al., 2009; Sripada et al., 2012; Tursich et al., 2015; Wu et al., 2011; Zhou et al., 2012). While these studies generally have many strengths, when used for the purpose of assessing ICNs, seed-based methods suffer from the constraints of having a limited number of regions-of-interest (ROIs). With only a limited number of ROIs, such approaches may not yield an optimal representation of the connectivity in the DMN as a whole. Further, the obtained results may be more prone to noise, since the metrics would be derived from few ROIs/connections, which could lead to false negatives (e.g., by missing important connections) and false positives (due to conclusions being drawn from non-representative connections). Heterogeneity in the choice of the seeds also limits comparison across studies. Although generalization is currently limited by such constraints, individuals with PTSD nonetheless appear to evidence decreased connectivity within the DMN (Akiki et al., 2017; Bluhm et al., 2009; DiGangi et al., 2016; Sripada et al., 2012; Tursich et al., 2015), though not without inconsistencies (Reuveni et al., 2016).

In addition to seed-based studies, our group and others have previously used network approaches to examine whole-brain functional connectivity, using voxel-based global brain connectivity (GBC), or other nodal metrics. These PTSD studies have sometimes identified

abnormalities in voxels/nodes that are known to be part of the DMN (e.g., decreased vmPFC nodal strength in PTSD), providing clues of DMN involvement (Abdallah et al., 2017b; Kennis et al., 2016; Koch et al., 2016; Lei et al., 2015; Patel et al., 2012; Suo et al., 2015). While these whole-brain studies have many strengths, a major limitation is the lack of ICN constraints, rendering the assessment of within-ICN topology impractical. The results therefore cannot be interpreted as being ICN-specific.

Considering the increased recognition of the role of ICN alterations in psychiatric disorders, and the need for developing circuit-based treatment (Kressel, 2017; Lui et al., 2016; Ross et al., 2017; Sheynin and Liberzon, 2016), it is critical for the field to develop tools to map ICN abnormalities. The accurate identification of ICN abnormalities could potentially pave the way for rational treatment development and target validation (Lanius et al., 2015). This has been recognized for brain stimulation approaches such as transcranial magnetic stimulation (Opitz et al., 2016), deep brain stimulation (Lozano and Lipsman, 2013), as well as for real time fMRI feedback (Garrison et al., 2013; Whitfield-Gabrieli et al., 2017), and psychotherapy (Lanius et al., 2015).

Meso-scale analysis of network architecture (e.g., communities) is well established in network science, and shifts the analysis to a scale coarser than seed-based and voxel/node-based whole-brain approaches (Fortunato, 2010; Meunier et al., 2010; Newman, 2011; Sporns and Betzel, 2016). Indeed, such methods have been used to define ICNs (e.g., (Power et al., 2011)). In the current study, we implemented an ICN-restricted approach to systematically investigate connectivity within the DMN. To achieve this goal, we used 1) a meta-analytically derived functional brain atlas from Power *et al* (2011) to delineate ROIs (also referred to as *nodes*); 2) a validated definition of the DMN using the ICN map from Yeo *et al* (2011); and 3) network tools from graph theory to probe connectivity patterns (Rubinov and Sporns, 2010). Here, it is important to note that the network-restricted methods established in the current study are not limited to a particular ICN or disease. Therefore, they can be easily implemented to investigate other circuits and neuropsychiatric disorders, extending the scientific benefit beyond the study's specific PTSD findings.

We hypothesized that PTSD symptoms would be associated with a pattern of network-wide connectivity dysfunction in the DMN. We aimed: 1) to determine whether previous observations made regarding altered DMN functional connectivity strength in PTSD hold true using a method that is DMN-specific, less model-reliant, and standardized (i.e., the DMN overall strength – the primary outcome of the study); 2) to further characterize DMN dysfunction in terms of network topology (i.e., the ability to integrate and segregate information); 3) to determine the modular architecture of the DMN, and to identify sub-communities relevant to PTSD; 4) to identify subregions in the DMN driving the network-wide abnormalities using edge-based statistics; 5) to determine, using data from diffusion MRI (dMRI), whether structural white matter abnormalities are driving the DMN functional abnormalities; and 6) to assess the robustness of results by repeating the analyses using alternate ROI definitions and network construction techniques. The main analyses were carried out with a dimensional approach based on a continuum of PTSD symptoms severity rather than diagnosis, consistent with the continuous nature of the disorder (further details in the Data in Brief supplements), but group comparisons were conducted also on the global

metrics to ascertain robustness and enable comparisons with other studies that have used group approaches.

2. Materials and Methods

This study is a novel analysis of a previously published data set (Abdallah et al., 2017b), however, none of the reported measures and analyses in the current report overlap with the previous study. Participants and clinical assessment details were previously reported (Abdallah et al., 2017b) and are also included in the accompanying data article (see online Data in Brief supplements). Written informed consents were obtained from all participants. The study was approved by Institutional Review Boards at Yale University and the VA Connecticut Healthcare System.

2.1 Neuroimaging Acquisition

Imaging data were collected using a Siemens TIM Trio 3.0 Tesla magnet with a 32-channel head coil. Three high-resolution structural MRI (sMRI) scans were used to improve surface delineation and enable subject-specific coregistration: 2 × T1-weighted MPRAGE (voxel size = 1 × 1 × 1 mm; TR = 2530 ms; TE = 2.71 ms; Flip = 7°); 1 × T2-weighted (voxel size = 1 × 1 × 1 mm; TR = 3200 ms; TE = 419 ms; Flip = 120°).

Whole-brain functional data were acquired using two 5-minute T2*-weighted BOLD resting-state runs (voxel size = 3.4 × 3.4 × 3.4 mm; TR = 25 ms; TE = 419 ms; Flip = 80°; 145 frames).

The diffusion MRI (dMRI) scan was acquired with a b-value of 1000 s/mm2, with 128 non-collinear encoding directions (voxel size = 1.7 × 1.7 × 3.0 mm; TR = 7400 ms; TE = 115 ms; Flip = 90°). The first image was acquired without diffusion weighting (b = 0 s/mm2).

2.2 First-level Processing

The preprocessing of resting-state fMRI consisted of correcting for motion and time-slice acquisition, brain extraction, spatial smoothing with 5 mm FWHM isotropic Gaussian kernel, high-pass temporal filtering (100 s), nonlinear registration of structural images to a standard Montreal Neurological Institute (MNI) template (2 × 2 × 2 mm), boundary-based registration (BBR) to high-resolution T1 images. In addition, we also performed motion scrubbing (Power et al., 2012) and regressed motion parameters, cerebrospinal fluid (CSF), white matter, the global brain signal, and their 1st derivatives (Power et al., 2014). Quality control criteria for each BOLD run were as follows: 1) no motion scrubbing greater than 50% of the run; and 2) no frame movement larger than 1 functional voxel.

Processing of dMRI scans was done using the *trac-all* pipeline in Freesurfer (Yendiki et al., 2011). The processing steps included eddy current and head motion estimation/correction (Yendiki et al., 2014), BBR registration of low-b diffusion (b = 0) to the high-resolution sMRI scans and registration to MNI template (1 × 1 × 1 mm), tensor estimation (*dtifit*), and the ball-and-stick model fit (*bedpostx*) (Behrens et al., 2003).

Tractography was performed by propagating 5000 streamline samples from each voxel using the FSL FDT toolbox (*probtrackx2*) (Behrens et al., 2007). Processing was conducted in the subject space.

CAPS scores were not correlated with head motion in the scanner during the fMRI [relative motion: $r_{(64)} = -0.0497$, $p = 0.6989$; absolute motion: $r_{(64)} = -0.1232$, $p = 0.3361$] or dMRI [translation motion: $r_{(60)} = 0.0445$; $p = 0.7355$; rotation motion: $r_{(60)} = 0.1324$; $p = 0.309$] scans.

2.3 Network Construction

Using a meta-analytically derived functional brain atlas from Power *et al* (which we refer to throughout as the functional atlas), we partitioned the brain into 264 cortical and subcortical ROIs (Power et al., 2011). To construct a DMN-specific network—and in order to avoid a potential bias in selecting the DMN component(s) post-signal decomposition— we decided to adopt a validated and reliable DMN mask established by Yeo *et al* (2011) (see online Data in Brief supplements for rationale). Of the original 264 ROIs, 64 ROIs were found to belong to the DMN map and were subsequently used for the analyses. See Figure 1 for a visual representation of the DMN nodes. We extracted and averaged time series from all voxels within each ROI. We then generated pairwise Pearson correlation coefficients from each ROI and proceeded to apply a Fischer z-transformation (Fz) to stabilize the correlation coefficient variance, resulting in a DMN-specific 64 × 64 Fz matrix. Each of the two 5-minute runs were processed separately until this point and then averaged prior to further analyses. Since it has been shown that regressing the global BOLD signal may induce anticorrelations, the interpretation of which remains unclear (Keller et al., 2013; Murphy et al., 2009), negative weights were initially discarded from analyses. However, the analyses were in part repeated with the complete networks (where both positive and negative weights are retained), on a post hoc basis to ensure consistency. Since certain graph theoretical measures such as the clustering coefficient require that weights fall between 0 and 1 (Onnela et al., 2005), Fz matrices were then rescaled by maximal weight ($Fz_{scaled} = Fz/max(abs(Fz))$; between 0 and 1 for the positive-only networks, and between - 1 and 1 for the full networks.

Concerns have been raised with regards to the reliability of weighted networks, namely that they are prone to noise (Kramer et al., 2009; Zalesky et al., 2016). To ascertain that our main results were not driven by this influence, we attempted two alternative approaches. In the first approach, we used stringent thresholding criteria (retaining the top 15% of the edges with the strongest weight) to attenuate the effect of such false positives. The second approach avoids such an arbitrary threshold and uses statistical significance to determine the presence of edges between nodes (Kramer et al., 2009). In addition to having the advantage of sparsifying the network in a principled way, such an approach may also reduce false negatives compared to highly stringent (arbitrary) cutoffs (Kramer et al., 2009). See Data in Brief article for details.

For the modularity analysis, we constructed a whole-sample average network. This representative network was constructed by taking the mean weight of each of the each of the entries in the 64 × 64 Fz matrices across the 65 participants. As with the networks in the

main analyses described above, negative values were discarded, and weights were rescaled between 0 and 1 for consistency.

Anatomical networks were constructed using the same parcellation as the functional networks (Power et al., 2011). Similar to the functional networks, we obtained a 64 × 64 DMN-specific anatomical connectivity matrix for each participant. Within each ROI, the number of streamlines passing through each voxel were log-transformed and averaged, and the matrix rescaled my maximal weight between 0 and 1 to maintain consistency with the functional networks). ROI volumes of the adopted functional atlas were uniform (10 mm diameter spheres), rendering normalization by ROI size unnecessary. As a quality control measure for the probabilistic tractography process, we calculated pairwise Pearson correlation values of the anatomical connectivity matrices across participants (values in the lower triangles were first transformed into a vector). The values of the correlations ranged from $r = 0.446$ to 0.758 with a mean of 0.612, indicating that the individual connections were consistent across individuals in the sample.

All analyses that follow were applied to the weighted matrices, using the weighted-variants of the functions included in the Brain Connectivity Toolbox (https://sites.google.com/site/bctnet) (Rubinov and Sporns, 2010, 2011), GenLouvain (Jeub et al., 2011–2017)(http://netwiki.amath.unc.edu/GenLouvain), and the Community Detection Toolbox (http://commdetect.weebly.com), under MATLAB 2016b (MathWorks Inc., Massachusetts, United States). Brain maps were generated using BrainNet Viewer (https://www.nitrc.org/projects/bnv) (Xia et al., 2013).

2.4 Connectivity Strength, Integration, and Segregation

As a primary outcome measure, we used the overall connectivity strength (S). We first calculated the nodal strength—the weighted variant of nodal degree, calculated as the sum of all neighboring link weights. When averaged across the network, it provides information about the overall connectivity strength or wiring investment of the network (Rubinov and Sporns, 2010).

We calculated two secondary global measures to further characterize information transfer across the network: global efficiency and clustering coefficient. Global efficiency measures network integration, the efficiency of overall network communication across the network. Mathematically, it is inversely related to the distance between nodes (i.e., the number of edges separating them, taking into account the weight of these edges) (Latora and Marchiori, 2001). The clustering coefficient measures network segregation by quantifying local interconnectivity. It is mathematically related to the number and weight of triangles formed by nodes and edges (Onnela et al., 2005; Watts and Strogatz, 1998). While the clustering coefficient is calculated on a nodal basis, an average across all nodes can be calculated and interpreted as a measure of overall network segregation—the capacity of specialized processing. All subsequent mentions of the clustering coefficient refer to the mean clustering coefficient across all nodes. Weighted generalizations of the clustering coefficient (Onnela et al., 2005), and the global efficiency (Latora and Marchiori, 2001; Rubinov and Sporns, 2010), were adopted for the calculations.

For a meaningful assessment of the global efficiency and clustering coefficient, the variability in overall connectivity strength S across subjects needs to be accounted for (Alexander-Bloch et al., 2010; van den Heuvel et al., 2017; van Wijk et al., 2010). One method to attenuate this variability consists of expressing variants of the global efficiency and clustering coefficient that have been normalized with matched random networks (van den Heuvel et al., 2017; van Wijk et al., 2010). Here we use this approach, with random networks that match the original networks in terms of degree and strength distribution (Maslov and Sneppen, 2002; Rubinov and Sporns, 2011). The normalized variants of the global efficiency and clustering coefficient were therefore defined as $E^{norm} = E^{original}/E^{random}$ and $C^{norm} = C^{original}/C^{random}$. It should be noted however that no method has been shown to be completely devoid of problems (van den Heuvel et al., 2017; van Wijk et al., 2010; Zalesky et al., 2012). For this reason, several other strategies were attempted and can be found in the accompanying online Data in Brief supplements.

Linear regressions were used to examine the relationship between CAPS scores and the global metrics. Details of group comparisons using general linear modes and robustness analyses can also be found in the online Data in Brief supplements.

2.5 Modular Organization

Briefly, we adopted a multi-iterative generalization of the Louvain community detection algorithm, with an association-reclustering approach, and applied it to our sample-average network (Blondel et al., 2008; Lancichinetti and Fortunato, 2012; Sporns and Betzel, 2016).

We optimized the modularity-like quality function Q (within-partition connectivity relative to between-partition connectivity) by running the Louvain algorithm iteratively until a plateau is reached and the largest level of modularity is achieved (Blondel et al., 2008; Newman and Girvan, 2004). Here a uniform null model rather than the more common Newman-Girvan null model was used, as it has been shown to be more suitable for correlation networks (Bazzi et al., 2016; Sporns and Betzel, 2016).

A resolution parameter γ can be used with the Louvain algorithm to control the number/size of detected communities. Rather than solely focusing on default modularity (i.e., for $\gamma = 1$), we explored a range of γ values (Betzel and Bassett, 2017; Betzel et al., 2013; Hric et al., 2014; Yang and Leskovec, 2015). Our goal was to identify a resolution at which the outputs of the Louvain algorithm were most stable (Traud et al., 2011), while retaining interpretability and plausibility with regard to the organization of the DMN (Andrews-Hanna et al., 2010). To achieve the latter, we made the decision to focus on partition solutions where the total number of detected communities was ≤ 6. We started with an arbitrary range for values of γ between 0.5 and 1.5, in increments of 0.01.

A shortcoming of modularity maximization methods is their degeneracy: they may output different partitions despite similar Q values (Good et al., 2010; Sporns and Betzel, 2016). Rather than adopt one of such outputs, we ran 200 randomly-seeded iterations of the algorithm (each optimized for Q), for each value of γ. We used the variability in the partition solutions to identify the candidate γ where the variability would be lowest, which we used as an indicator of the presence of well-defined communities at this resolution

(Betzel and Bassett, 2017; Doron et al., 2012). To quantify partition solution similarity, we used the Rand index (Traud et al., 2011). For each value of γ, z-scored Rand indices were calculated on a pairwise basis from the 200 partition solutions, and then averaged. We then selected the γ value corresponding to the maximal z-Rand value, in the range of γ values resulting in ≤ 6 total number of detected communities (Figure 2).

To resolve the variability across the 200 partition solutions, an association-reclustering approach was used to reach consensus (Lancichinetti and Fortunato, 2012). We generated a 64 × 64 agreement matrix D from the 200 partition solutions. D was constructed such as each cell indicates the probability that nodes were assigned to the same community, and was therefore weighted (Sporns and Betzel, 2016). Without thresholding, the Louvain algorithm was run on D for another 200 iterations, to verify that an identical partitioning solution has been reached. Here we used the commonly used permutation null model (Lancichinetti and Fortunato, 2012; Sporns and Betzel, 2016). It should be noted however, that in some cases applying a threshold to D and/or repeated meta-association-reclustering steps are necessary to converge onto a stable partition (Sporns and Betzel, 2016); we found this to be unnecessary in our case, likely due to the relatively high consistency among the partition solutions.

2.6 Modularity and PTSD Severity

In addition to identifying the functional modular organization of the DMN in our sample (Figure 3), our interest was in determining whether modularity is associated with PTSD symptom severity. We moved back to the subject level, and used the partition solution that we identified above to calculate the modularity Q for each subject, in an approach adopted from (Betzel et al., 2014).

However, modular organization is known to be affected by the overall level of connectedness of the network (Fortunato and Barthelemy, 2007). To inform whether the relationship between subject-specific modularity and PTSD symptom severity is driven by this phenomenon, we examined the relationship between Q and S.

To try to obtain meaningful results at the level of the individual communities despite a potential systematic bias due to overall DMN connectivity differences, we calculated a ratio of the within-community strength to S for each. The relationship between these ratios and PTSD symptom severity was examined using linear regressions, and FDR was used to control for multiple comparisons.

2.7 Edge Statistical Testing

Another approach to we used to map abnormalities observed on the whole-network level to a finer scale consisted of statistically testing all edges in the networks— [N × (N − 1)/2] = 2,016 edges in this case, while correcting for family-wise error. The DMN connectivity matrices of each participant were entered as dependent variables and the total CAPS score was used as a predictor variable (connection threshold $t = 3.5$; permutations = 10,000; corrected $\alpha < 0.05$). Network-based statistics (NBS) were used to control for family-wise error at the subnetwork level (Zalesky et al., 2010). Robustness analyses can be found in the online Data in Brief supplements.

2.8 Anatomical Connectivity

Highly informative observations have been recently made regarding the relationship between functional and structural networks obtained from the same individuals (Betzel et al., 2013; Goni et al., 2014; Honey et al., 2009; Mišić et al., 2016). However, the scope of our analysis here is limited to assessing whether there is evidence of a direct parallel between white matter dysconnectivity and the functional abnormalities that we identified in this sample, and so are focused and post hoc in nature. These analyses included a subsample of individuals with both fMRI and dMRI scans (n = 61).

A linear regression was used to assess the relationship between structural connectivity strength (the structural equivalent of S) and CAPS. To test whether the frontal dysconnectivity evidenced in the functional edge analysis was associated (e.g., potentially mediated) by white matter structural connectivity, we tested these functionally abnormal edges/nodes in structural networks using NBS. To increase sensitivity, we reduced multiple comparisons by only including the edges/nodes that were detected with the functional NBS analysis.

2.10 Robustness of Global Measures

In order to assess the robustness of our global metrics and ascertain that the detected changes were not due to intricacies of the employed network construction method, we conducted additional robustness analyses using alternate node (HCP multi-modal atlas), edge (signed, thresholded, statistically significant), and DMN definitions (Glasser et al., 2016; Kramer et al., 2009; Power et al., 2011; van den Heuvel et al., 2017). Details can be found in the online Data in Brief supplements.

3. Results

Our sample was, on average, comprised of Veterans with moderate to severe PTSD severity [mean CAPS = 43.4 (SEM = 3.7)], but included individuals that spanned the whole spectrum of the disease, with 54% meeting DSM-IV criteria for PTSD diagnosis. The mean age was 34.8 (SEM = 1.2), and the participants were predominately male (89%). Additional demographics and behavioral details can be found in the online Data in Brief supplements.

3.1 Connectivity Strength, Integration, and Segregation

For our primary measure, we found evidence of reduced functional connectivity strength (S) within the DMN in participants with high PTSD symptom severity [$r_{(64)} = -0.329$, $p = 0.0075$; Figure 4A]. Similarly, group comparisons revealed a lower S in subjects who met DSM-IV criteria for PTSD compared to those who did not (i.e., combat controls): [combat controls (CC): mean = 10.30 ± 0.31; PTSD: mean = 9.23 ± 0.28; $p = 0.014$; Figure 4B].

As for the secondary global measures, we found reduced global efficiency [E^{norm}: $r_{(64)} = -0.299$, $p = 0.0157$; Figure 5A], and increased overall clustering coefficient [C^{norm}: $r_{(64)} = 0.334$, $p = 0.0065$; Figure 5B] in participants with high PTSD symptom severity. Similarly, group comparisons revealed a lower E^{norm} but higher C^{norm} in subjects who met DSM-IV criteria for PTSD compared to those who did not: E^{norm} [CC: mean = 0.892 ± 0.004; PTSD:

mean = 0.877 ± 0.004; $p = 0.01$; Figure 5C], and C^{norm} [CC: mean = 1.067 ± 0.009; PTSD: mean = 1.097 ± 0.008; $p = 0.016$; Figure 5D].

Controlling for various behavioral and epidemiological potential confounds did not change the pattern of the results. None of the PTSD subscale scores were significant as part of a multivariable regression when explored with S, E^{norm}, or C^{norm} ($p > 0.15$ in all cases). Combat exposure severity did not correlate with any of the connectivity measures, nor was the interaction with CAPS significant ($p > 0.4$ in all cases). For details, see online Data in Brief supplements.

3.2 Modularity

The highest average z-Rand score was identified at $\gamma = 1.26$ (Figure 2). Applying the association-reclustering procedure to the ensemble of 200 partition solutions at this resolution yielded a consensus partition with 4 communities (Figure 3). The divisions were as follows: a posterior community (PCC, precuneus, and left angular gyrus), a frontal community (vmPFC and dmPFC), an MT-P community (middle temporal and parahippocampal cortex), and an MT-IF (middle temporal and inferior frontal cortex) community.

Moving back from the average network to the individuals' networks, we were interested in exploring whether PTSD symptom severity was associated with modularity. There was a trend-level significance for the regression between the total modularity Q and CAPS [$r_{(64)} = 0.252$, $p = 0.0430$]. Yet, there was also a strong inverse correlation between Q and S [$r_{(64)} = -0.677$, $p < 0.0001$], raising the possibility that an increase in modularity may be driven by loss of connectivity in the DMN (described under *3.1*).

To try to obtain more meaningful results at the level of the communities and assess whether particular communities were driving the decrease in overall strength, for each of the 4 modules, we calculated a ratio of the within-module strength to S. Here we found that $S_{posterior}/S$ was positively correlated with CAPS [$r_{(64)} = 0.346$, corrected $p = 0.019$; FDR adjusted for 4 comparisons], but no correlation was evident between $S_{frontal}/S$ [$r_{(64)} = -0.007$, corrected $p = 0.955$; FDR adjusted], S_{MT}/S [$r_{(64)} = 0.116$, corrected $p = 0.609$; FDR adjusted], or $S_{MT\text{-}IF}/S$ [$r_{(64)} = 0.094$, corrected $p = 0.609$; FDR adjusted] and CAPS.

Totals for within-community and between-community strengths were both negatively correlated with CAPS [S_{within}: $r_{(64)} = -309$, $p = 0.0124$; $S_{between}$: $r_{(64)} = -0.314$, $p = 0.0110$].

3.3 Edge Statistical Testing

After correcting for family-wise error using NBS, analyses at the level of the whole DMN identified a total of 6 abnormal edges and 7 nodes, with connection weights that were negatively associated with PTSD severity (Figure 6). Out of the 6 abnormal edges, all involve the PFC [mPFC and lateral orbitofrontal cortex (lOFC)]. No edges were found to be positively associated with PTSD severity. More details can be found in the online Data in Brief supplements.

3.4 Anatomical Connectivity

No statistically significant relationship was found between CAPS and structural strength [$r_{(60)} = -0.136$, $p = 0.2906$]. A positive correlation was found between structural strength and functional strength [$r_{(60)} = 0.288$, $p = 0.0234$]. To ensure that this was not a false-negative finding due to the suboptimal functional brain atlas, the dMRI networks were reconstructed with the HCP multi-modal atlas (normalized by ROI volume), here too, no statistically significant relationship was found [*S:* $r_{(60)} = -0.127$, $p = 0.335$].

To test whether the PFC functional dysconnectivity identified using NBS is driven by a disruption in structural connectivity, we tested these functionally abnormal edges/nodes in structural networks using NBS, in the subset of patients having completed both fMRI and dMRI scans (n = 61). None of the structural edges were found to be associated with CAPS.

3.5 Robustness of Global Measures

The calculations of the global measures (S, E^{norm}, and C^{norm}) using the different node and edge definitions revealed a largely similar pattern of results. The primary outcome measure S was consistently negatively correlated with CAPS scores. Details can be found in the online Data in Brief supplements.

4. Discussion

Consistent with the study aims, we established measures of ICN connectivity, and tested their utility in identifying a DMN endophenotype of PTSD symptom psychopathology. Confirming our hypothesis, the results provide evidence of altered functional connectivity in the DMN of Veterans with high PTSD symptom severity. While we opted for a single group dimensional analysis for our primary analyses (see Data in Brief supplements for justification), we also compared the global measures between PTSD and non-PTSD subjects, this was done to ensure the robustness of the results, and to enable a meaningful comparison between our results and those of other studies that follow a group comparison approach. To this aim, we divided our sample into two groups: those who met DSM-IV criteria for PTSD and those who did not, i.e., combat exposed controls.

Our primary measure of DMN overall functional connectivity strength S was negatively correlated with symptom severity. Consistent with the correlational analysis, we found that the PTSD group was characterized with a decreased S, compared to the non-PTSD combat exposed group. These findings extend prior evidence from seed-based studies showing a seed-to-seed decreased connectivity in PTSD (Bluhm et al., 2009; DiGangi et al., 2016; Miller et al., 2017a; Sripada et al., 2012; Tursich et al., 2015). Compared to seed connectivity, S may be more robust in assessing ICNs as it leverages connectivity from the whole ICN, rather than being based on a few seeds only. For the same reason, it may lead to more reproducible results, as S is less likely to be influenced by small perturbations (e.g., alignment, or other localized noise issues) given that it is calculated from diversified nodes (e.g., 64 in this study). For example, a recent study examined within-DMN functional connectivity but failed to demonstrate DMN alterations in the PTSD group (Reuveni et al., 2016). However, only 4 DMN seeds (mPFC, precuneus, inferior parietal lobules bilaterally)

were used to explore connectivity between these ROIs and a DMN map decomposed on a subject-specific basis. The reliance on a small number of nodes could have resulted in a decreased sensitivity to detect differences. By adopting a 64-node functionally-derived map for the DMN, we have taken a step towards less model-dependence (e.g., using seeds in the mPFC or PCC as a surrogate for the DMN), while avoiding the shortcomings of a sample- or subject-specific DMN decomposition.

With regard to the secondary measures of global topology, the normalized global efficiency E^{norm} was negatively correlated with PTSD symptom severity, while the clustering coefficient C^{norm} was positively correlated. Here too, the results of the group comparisons were consistent with the correlation analyses: the PTSD group was characterized by lower E^{norm} and higher C^{norm} compared to the non-PTSD combat exposed group. These topological alterations may represent an overall loss of integration (global efficiency) and increased segregation (clustering coefficient) of the DMN with increasing PTSD severity. This finding could reflect a tendency of increased regional specialization where local interconnections would be expected to be augmented at the expense of integrative long-range connections. Taken together, these findings could represent a deviation from the optimal cost-effective connectivity pattern (Bassett and Bullmore, 2016). The DMN plays an important role in internal mentation and self-directed thought. This disrupted connectivity may reflect a reduced ability to maintain a tranquil state of internal mentation due to increased arousal and intrusive and negative thoughts that is observed in PTSD (Abdallah et al., 2017a).

In the current study, we explored modularity at different scales and selected scale that yielded the most stable (similar) partitioning solutions. In the consensus partition we adopted, the DMN was partitioned into 4 communities: (1) posterior, comprising the PCC, precuneus, and left angular gyrus; (2) frontal, comprising nodes in the vmPFC and dmPFC; (3) MT-P, comprising parts of the middle temporal and parahippocampal cortex; and MT-IF, comprising parts of the middle temporal and inferior frontal cortex. Interestingly, although the division into frontal, posterior, and MT is consistent with recent evidence from functional and structural studies that suggest that the DMN comprises distinct subsystems, our analysis suggested a division of the MT into MT-P and MT-IF (Andrews-Hanna et al., 2010; Yeo et al., 2011). It remains unclear whether this is due to differences in network definitions/preprocessing or in the sample (healthy vs. all combat-combat exposed and in part with PTSD diagnosis). Adopting a coarser resolution (γ = [0.6–0.8]) would have yielded 3 communities, more consistent with such earlier studies, but was markedly less stable than the 4-community solution (see Figure 2). This partition solution was applied to the individual networks. A statistically significant correlation was present between PTSD symptom severity and the total modularity Q, although this might have been driven by the difference in S. After calculating the ratio of the strength within each of the communities to total S, we were able to find that connectivity within the posterior community (PCC, precuneus) may have been spared relative to the decreased connectivity strength in the rest of the DMN. Breaking up S into within- and between-community connectivity strength shows that both contribute similar variances (9.5% and 9.8% respectively) to PTSD symptom severity.

The results of our whole-DMN NBS analyses suggests that in PTSD the PFC may be characterized by loss of connectivity with the rest of the DMN: all impaired edges (edge strength negatively correlated with symptom severity) involved the mPFC or lOFC. The dysconnectivity between the mPFC and lOFC node (Figure 6) may be of particular clinical relevance to PTSD, since the lOFC is known to relay sensory input to the mPFC and support stimulus-value associations (Euston et al., 2012). lOFC-mPFC dysconnectivity may therefore reflect this system's impaired ability to support cognitive reappraisal. Task fMRI studies have implicated the mPFC in self-judgment and assessing personal significance (Heatherton et al., 2006; Mitchell et al., 2006). It is therefore possible that abnormalities in this area are linked to the pervasive negative thoughts often present in PTSD. These localized findings may be relevant for future circuit-based brain stimulation treatments (Karsen et al., 2014; Nahas et al., 2010; Opitz et al., 2016; Sheynin and Liberzon, 2016). The characterization of the meso-scale network architecture in disease may also have translational value beyond guiding brain stimulation applications (Lanius et al., 2015). Other approaches that enable the manipulation of ICN-level activity are currently in development (Garrison et al., 2013; Whitfield-Gabrieli et al., 2017). Another possible application could be the potential for specificity of DMN biomarkers in particular. While in this study we have identified a loss of connectivity in the DMN that is associated with PTSD, the opposite pattern of DMN connectivity, i.e., strengthening of DMN connectivity has been described in major depressive disorder (Mulders et al., 2015). Accurate characterization can in the future pave way for more fine-grained investigations aimed at predicting disease-specific treatment response and the identification of at-risk individuals (e.g., using longitudinal data).

Using dMRI data from the same subjects, anatomical connectivity strength within the DMN was positively correlated with functional connectivity strength (consistent with prior evidence (Honey et al., 2009)), but was not found to be significantly associated with PTSD severity. Edges identified in the functional NBS analyses were also not found to be associated with PTSD symptom severity. These findings suggest that the abnormalities may be confined to the functional level, rather than being due to underlying white matter dysconnectivity (e.g., conditions such as traumatic brain injury (Eierud et al., 2014)). Though it should be noted that there remains a possibility of more complex interactions, to be thoroughly explored in future studies.

Recognizing the potential variability due to the choice of atlas and network construction method, we repeated our analyses of the global topological measures using networks constructed with alternate definitions. As alternate node definition, we used a state of the art multi-modal cortical parcellation (Glasser et al., 2016). We also attempted various edge definitions: signed full, sparse thresholded (15% density), and statistically significant networks (Kramer et al., 2009). We obtained a largely similar pattern of results for our global topological metrics (see online Data in Brief supplements). DMN overall strength S was more robust than global efficiency and clustering coefficient. This apparent robustness in our method affirms its potential utility as a biomarker, although the specificity and sensitivity of these findings to PTSD remains to be fully assessed. This will necessitate a systematic examination of the DMN across different neuropsychiatric disorders or clusters of symptoms using similar methods, and in other PTSD samples to assess replicability.

Limitations and future directions

Limitations in the current study design include its cross-sectional nature, which prevents conclusions as to whether altered DMN connectivity represents a vulnerability for developing PTSD in response to trauma, or whether these changes are trauma-induced. The decision not to exclude comorbid psychiatric and substance abuse disorders, mild TBI, and psychotropic medications limits internal validity, although it enhances external validity by rendering our sample closer to the Veterans PTSD population. We attempted to ensure that these confounds did not drive the results by conducting analyses with a subgroup of non-medicated subjects, and subgroup of subjects with no psychiatric comorbidities. We also covaried for these confounds in post hoc tests. The results remained consistent with the full group analyses and can be found in the Data in Brief supplements. However, we recognize that this issue remains a significant limitation that can only be thoroughly addressed in samples consisting of non-comorbid and non-medicated individuals. The absence of a non-combat-exposed healthy control group limits the conclusions drawn to the combat-exposed population. Women comprised only 11% of the total sample, which limits generalizability of the results to that group. The primary outcome of the study was *S,* while all other analyses are secondary in nature. Therefore, it should be noted that the secondary analyses were often not adjusted for the number of comparisons across methods and they should therefore be interpreted in this context (the modularity and edge-wise analyses were each adjusted internally: 4 comparisons for modularity and 2016 comparisons for edge-wise statistics). Moreover, while putative confounds of functional connectivity (e.g., motion artifacts) were addressed in the processing pipeline, and a systematic bias in in-scanner movement is unlikely (see *2.2*), there remains a possibility that other currently unknown confounds are at play.

Other limitations regarding the functional networks should be mentioned. First, fMRI-derived networks are known to be noisy and can be affected by non-trivial choices in the network construction process, and to date, there's no consensus on the optimal method (Fornito et al., 2015; Kramer et al., 2009; van den Heuvel et al., 2017; Zalesky et al., 2016). Although we used several different alternate methods to demonstrate relative robustness, this was by no means comprehensive as there remains other methods that could be assessed in the future. A limitation specific to the global efficiency and clustering coefficient is that the effect of S should be removed prior to assessing them (otherwise the varying level of S across individuals may bias their calculation). Here we reported the results obtained using the normalization method with a null model that preserves the weight and degree distribution (Maslov and Sneppen, 2002; Rubinov and Sporns, 2010; van den Heuvel et al., 2017), since it was the one that appropriately mitigated this effect (a detailed analysis can be found in the Data in Brief supplements). The appropriateness of such null models has been recently put into question (Zalesky et al., 2012); these concerns appear to be specific to making empirical observations as they may lead to exaggerated small-world properties in the networks. Although in this study we make no such observations and we only use them to account for the difference in connectivity, improved null models should be developed in the future to confirm these results. The asymmetrical findings in the left mPFC and lOFC needs to be fully assessed. Differences in both hemispheres have been reported in the literature (Kennis et al., 2015; Patel et al., 2012; Yamasue et al., 2003). Therefore, it remains to be seen if this

asymmetry represents true lateralization of function (e.g., left vmPFC is linked to emotional appraisal (Etkin and Schatzberg, 2011)).

Acknowledgments

Funding

Funding support was provided by the U.S. Department of Veterans Affairs National Center for PTSD, NIH (MH-101498), and the Brain and Behavior Foundation (NARSAD). Dr. Scott's participation was supported by a Department of Veterans Affairs Career Development Award (IK2CX000772). Support for Dr. L. A. Averill was provided by a Brain & Behavior Research Foundation (NARSAD) Young Investigator Award and the NY Women's Committee who named Dr. L. A. Averill as the Woman of the Year Breaking the Silence Against Mental Illness and by a Department of Veterans Affairs VISN 1 Career Development Award. The content is solely the responsibility of the authors and does not necessarily represent the official views of the sponsors. The sponsors had no role in the design and conduct of the study; collection, management, analysis, and interpretation of the data; and preparation, review, or approval of the manuscript. Dr. Abdallah has served as a consultant or on advisory boards for Genentech and Janssen. He also serves as editor for the journal Chronic Stress published by SAGE Publications, Inc. Dr. Krystal is a consultant for AbbVie, Inc., Amgen, Astellas Pharma Global Development, Inc., AstraZeneca Pharmaceuticals, Biomedisyn Corporation, Bristol-Myers Squibb, Eli Lilly and Company, Euthymics Bioscience, Inc., Neurovance, Inc., FORUM Pharmaceuticals, Janssen Research & Development, Lundbeck Research USA, Novartis Pharma AG, Otsuka America Pharmaceutical, Inc., Sage Therapeutics, Inc., Sunovion Pharmaceuticals, Inc., and Takeda Industries; is on the Scientific Advisory Board for Lohocla Research Corporation, Mnemosyne Pharmaceuticals, Inc., Naurex, Inc., and Pfizer; is a stockholder in Biohaven Medical Sciences; holds stock options in Mnemosyne Pharmaceuticals, Inc.; holds patents for Dopamine and Noradrenergic Reuptake Inhibitors in Treatment of Schizophrenia, U.S. Patent No. 5,447,948 (issued Sep 5, 1995), and Glutamate Modulating Agents in the Treatment of Mental Disorders, U.S. Patent No. 8,778,979 (issued Jul 15, 2014); and filed a patent for Intranasal Administration of Ketamine to Treat Depression. U.S. Application No. 14/197,767 (filed on Mar 5, 2014); U.S. application or Patent Cooperation Treaty international application No. 14/306,382 (filed on Jun 17, 2014).

The authors would like to thank the Veterans who participated in this study for their invaluable contribution, and the reviewers for their helpful comments on an earlier version of the manuscript.

References

Abdallah CG, Southwick SM, Krystal JH. Neurobiology of posttraumatic stress disorder (PTSD): A path from novel pathophysiology to innovative therapeutics. Neuroscience Letters. 2017a; 649:130–132. [PubMed: 28478864]

Abdallah CG, Wrocklage KM, Averill CL, Akiki T, Schweinsburg B, Roy A, Martini B, Southwick SM, Krystal JH, Scott JC. Anterior hippocampal dysconnectivity in posttraumatic stress disorder: a dimensional and multimodal approach. Transl Psychiatry. 2017b; 7:e1045. [PubMed: 28244983]

Akiki TJ, Averill CL, Abdallah CG. A Network-Based Neurobiological Model of PTSD: Evidence From Structural and Functional Neuroimaging Studies. Current Psychiatry Reports. 2017; 19:81. [PubMed: 28924828]

Alexander-Bloch AF, Gogtay N, Meunier D, Birn R, Clasen L, Lalonde F, Lenroot R, Giedd J, Bullmore ET. Disrupted modularity and local connectivity of brain functional networks in childhood-onset schizophrenia. Front Syst Neurosci. 2010; 4:147. [PubMed: 21031030]

Andrews-Hanna JR, Reidler JS, Sepulcre J, Poulin R, Buckner RL. Functional-anatomic fractionation of the brain's default network. Neuron. 2010; 65:550–562. [PubMed: 20188659]

Bassett DS, Bullmore ET. Small-World Brain Networks Revisited. Neuroscientist. 2016

Bazzi M, Porter MA, Williams S, McDonald M, Fenn DJ, Howison SD. Community Detection in Temporal Multilayer Networks, with an Application to Correlation Networks. Multiscale Modeling & Simulation. 2016; 14:1–41.

Behrens TE, Berg HJ, Jbabdi S, Rushworth MF, Woolrich MW. Probabilistic diffusion tractography with multiple fibre orientations: What can we gain? NeuroImage. 2007; 34:144–155. [PubMed: 17070705]

Behrens TE, Woolrich MW, Jenkinson M, Johansen-Berg H, Nunes RG, Clare S, Matthews PM, Brady JM, Smith SM. Characterization and propagation of uncertainty in diffusion-weighted MR imaging. Magn Reson Med. 2003; 50:1077–1088. [PubMed: 14587019]

Betzel RF, Bassett DS. Multi-scale brain networks. NeuroImage. 2017; 160:73–83. [PubMed: 27845257]

Betzel RF, Byrge L, He Y, Goni J, Zuo XN, Sporns O. Changes in structural and functional connectivity among resting-state networks across the human lifespan. NeuroImage. 2014; 102:345–357. [PubMed: 25109530]

Betzel RF, Griffa A, Avena-Koenigsberger A, GoNI J, Thiran JP, Hagmann P, Sporns O. Multi-scale community organization of the human structural connectome and its relationship with resting-state functional connectivity. Network Science. 2013; 1:353–373.

Blondel VD, Guillaume J-L, Lambiotte R, Lefebvre E. Fast unfolding of communities in large networks. Journal of Statistical Mechanics: Theory and Experiment. 2008

Bluhm RL, Williamson PC, Osuch EA, Frewen PA, Stevens TK, Boksman K, Neufeld RW, Theberge J, Lanius RA. Alterations in default network connectivity in posttraumatic stress disorder related to early-life trauma. J Psychiatry Neurosci. 2009; 34:187–194. [PubMed: 19448848]

Buckner RL, Andrews-Hanna JR, Schacter DL. The brain's default network: anatomy, function, and relevance to disease. Ann N Y Acad Sci. 2008; 1124:1–38. [PubMed: 18400922]

Damoiseaux JS, Rombouts SA, Barkhof F, Scheltens P, Stam CJ, Smith SM, Beckmann CF. Consistent resting-state networks across healthy subjects. Proc Natl Acad Sci U S A. 2006; 103:13848–13853. [PubMed: 16945915]

Daniels JK, Frewen P, McKinnon MC, Lanius RA. Default mode alterations in posttraumatic stress disorder related to early-life trauma: a developmental perspective. J Psychiatry Neurosci. 2011; 36:56–59. [PubMed: 20964955]

DiGangi JA, Tadayyon A, Fitzgerald DA, Rabinak CA, Kennedy A, Klumpp H, Rauch SA, Phan KL. Reduced default mode network connectivity following combat trauma. Neurosci Lett. 2016; 615:37–43. [PubMed: 26797653]

Doron KW, Bassett DS, Gazzaniga MS. Dynamic network structure of interhemispheric coordination. Proceedings of the National Academy of Sciences. 2012; 109:18661–18668.

Eierud C, Craddock RC, Fletcher S, Aulakh M, King-Casas B, Kuehl D, LaConte SM. Neuroimaging after mild traumatic brain injury: Review and meta-analysis(). NeuroImage: Clinical. 2014; 4:283–294. [PubMed: 25061565]

Etkin A, Schatzberg AF. Common abnormalities and disorder-specific compensation during implicit regulation of emotional processing in generalized anxiety and major depressive disorders. Am J Psychiatry. 2011; 168:968–978. [PubMed: 21632648]

Euston DR, Gruber AJ, McNaughton BL. The Role of Medial Prefrontal Cortex in Memory and Decision Making. Neuron. 2012; 76:1057–1070. [PubMed: 23259943]

Fornito A, Zalesky A, Breakspear M. The connectomics of brain disorders. Nat Rev Neurosci. 2015; 16:159–172. [PubMed: 25697159]

Fortunato S. Community detection in graphs. Physics Reports. 2010; 486:75–174.

Fortunato S, Barthelemy M. Resolution limit in community detection. Proceedings of the National Academy of Sciences. 2007; 104:36–41.

Garrison KA, Scheinost D, Worhunsky PD, Elwafi HM, Thornhill TAt, Thompson E, Saron C, Desbordes G, Kober H, Hampson M, Gray JR, Constable RT, Papademetris X, Brewer JA. Real-time fMRI links subjective experience with brain activity during focused attention. NeuroImage. 2013; 81:110–118. [PubMed: 23684866]

Glasser MF, Coalson TS, Robinson EC, Hacker CD, Harwell J, Yacoub E, Ugurbil K, Andersson J, Beckmann CF, Jenkinson M, Smith SM, Van Essen DC. A multi-modal parcellation of human cerebral cortex. Nature. 2016; 536:171–178. [PubMed: 27437579]

Goni J, van den Heuvel MP, Avena-Koenigsberger A, Velez de Mendizabal N, Betzel RF, Griffa A, Hagmann P, Corominas-Murtra B, Thiran JP, Sporns O. Resting-brain functional connectivity predicted by analytic measures of network communication. Proceedings of the National Academy of Sciences. 2014; 111:833–838.

Good BH, de Montjoye YA, Clauset A. Performance of modularity maximization in practical contexts. Physical Review E. 2010; 81:046106.

Heatherton TF, Wyland CL, Macrae CN, Demos KE, Denny BT, Kelley WM. Medial prefrontal activity differentiates self from close others. Soc Cogn Affect Neurosci. 2006; 1:18–25. [PubMed: 18985097]

Honey CJ, Sporns O, Cammoun L, Gigandet X, Thiran JP, Meuli R, Hagmann P. Predicting human resting-state functional connectivity from structural connectivity. Proceedings of the National Academy of Sciences. 2009; 106:2035–2040.

Hric D, Darst RK, Fortunato S. Community detection in networks: Structural communities versus ground truth. Physical Review E. 2014; 90:062805.

Jeub LG, Bazzi M, Jutla IS, Mucha PJ. A generalized Louvain method for community detection implemented in MATLAB. 2011–2017

Karsen EF, Watts BV, Holtzheimer PE. Review of the effectiveness of transcranial magnetic stimulation for post-traumatic stress disorder. Brain Stimul. 2014; 7:151–157. [PubMed: 24486424]

Keller CJ, Bickel S, Honey CJ, Groppe DM, Entz L, Craddock RC, Lado FA, Kelly C, Milham M, Mehta AD. Neurophysiological investigation of spontaneous correlated and anticorrelated fluctuations of the BOLD signal. J Neurosci. 2013; 33:6333–6342. [PubMed: 23575832]

Kennis M, Rademaker AR, van Rooij SJH, Kahn RS, Geuze E. Resting state functional connectivity of the anterior cingulate cortex in veterans with and without post-traumatic stress disorder. Human brain mapping. 2015; 36:99–109. [PubMed: 25137414]

Kennis M, van Rooij SJ, van den Heuvel MP, Kahn RS, Geuze E. Functional network topology associated with posttraumatic stress disorder in veterans. Neuroimage Clin. 2016; 10:302–309. [PubMed: 26900570]

Koch SB, van Zuiden M, Nawijn L, Frijling JL, Veltman DJ, Olff M. Aberrant Resting-State Brain Activity in Posttraumatic Stress Disorder: A Meta-Analysis and Systematic Review. Depress Anxiety. 2016; 33:592–605. [PubMed: 26918313]

Kramer MA, Eden UT, Cash SS, Kolaczyk ED. Network inference with confidence from multivariate time series. Physical Review E. 2009; 79:061916.

Kressel HY. Setting Sail: 2017. Radiology. 2017; 282:4–6. [PubMed: 28005504]

Laird AR, Fox PM, Eickhoff SB, Turner JA, Ray KL, McKay DR, Glahn DC, Beckmann CF, Smith SM, Fox PT. Behavioral interpretations of intrinsic connectivity networks. J Cogn Neurosci. 2011; 23:4022–4037. [PubMed: 21671731]

Lancichinetti A, Fortunato S. Consensus clustering in complex networks. Scientific Reports. 2012; 2:336. [PubMed: 22468223]

Lanius RA, Bluhm RL, Coupland NJ, Hegadoren KM, Rowe B, Theberge J, Neufeld RW, Williamson PC, Brimson M. Default mode network connectivity as a predictor of post-traumatic stress disorder symptom severity in acutely traumatized subjects. Acta Psychiatr Scand. 2010; 121:33–40. [PubMed: 19426163]

Lanius RA, Frewen PA, Tursich M, Jetly R, McKinnon MC. Restoring large-scale brain networks in PTSD and related disorders: a proposal for neuroscientifically-informed treatment interventions. European Journal of Psychotraumatology. 2015; 6:10. 3402/ejpt.v3406.27313.

Latora V, Marchiori M. Efficient behavior of small-world networks. Phys Rev Lett. 2001; 87:198701. [PubMed: 11690461]

Lei D, Li K, Li L, Chen F, Huang X, Lui S, Li J, Bi F, Gong Q. Disrupted Functional Brain Connectome in Patients with Posttraumatic Stress Disorder. Radiology. 2015; 276:818–827. [PubMed: 25848901]

Lozano, Andres M., Lipsman, N. Probing and Regulating Dysfunctional Circuits Using Deep Brain Stimulation. Neuron. 2013; 77:406–424. [PubMed: 23395370]

Lui S, Zhou XJ, Sweeney JA, Gong Q. Psychoradiology: The Frontier of Neuroimaging in Psychiatry. Radiology. 2016; 281:357–372. [PubMed: 27755933]

Maslov S, Sneppen K. Specificity and stability in topology of protein networks. Science. 2002; 296:910–913. [PubMed: 11988575]

Meunier D, Lambiotte R, Bullmore ET. Modular and Hierarchically Modular Organization of Brain Networks. Frontiers in Neuroscience. 2010; 4:200. [PubMed: 21151783]

Miller DR, Hayes SM, Hayes JP, Spielberg JM, Lafleche G, Verfaellie M. Default Mode Network Subsystems Are Differentially Disrupted in Posttraumatic Stress Disorder. Biological Psychiatry: Cognitive Neuroscience and Neuroimaging. 2017a; 2:363–371. [PubMed: 28435932]

Miller DR, Logue MW, Wolf EJ, Maniates H, Robinson ME, Hayes JP, Stone A, Schichman S, McGlinchey RE, Milberg WP, Miller MW. Posttraumatic stress disorder symptom severity is associated with reduced default mode network connectivity in individuals with elevated genetic risk for psychopathology. Depression and Anxiety. 2017b; 34:632–640. [PubMed: 28494120]

Mišić B, Betzel RF, de Reus MA, van den Heuvel MP, Berman MG, McIntosh AR, Sporns O. Network-Level Structure-Function Relationships in Human Neocortex. Cerebral Cortex. 2016; 26:3285–3296. [PubMed: 27102654]

Mitchell JP, Macrae CN, Banaji MR. Dissociable medial prefrontal contributions to judgments of similar and dissimilar others. Neuron. 2006; 50:655–663. [PubMed: 16701214]

Mulders PC, van Eijndhoven PF, Schene AH, Beckmann CF, Tendolkar I. Resting-state functional connectivity in major depressive disorder: A review. Neuroscience & Biobehavioral Reviews. 2015; 56:330–344. [PubMed: 26234819]

Murphy K, Birn RM, Handwerker DA, Jones TB, Bandettini PA. The impact of global signal regression on resting state correlations: are anti-correlated networks introduced? NeuroImage. 2009; 44:893–905. [PubMed: 18976716]

Nahas Z, Anderson BS, Borckardt J, Arana AB, George MS, Reeves ST, Takacs I. Bilateral Epidural Prefrontal Cortical Stimulation for Treatment-Resistant Depression. Biological Psychiatry. 2010; 67:101–109. [PubMed: 19819427]

Newman MEJ. Communities, modules and large-scale structure in networks. Nature Physics. 2011; 8:25.

Newman MEJ, Girvan M. Finding and evaluating community structure in networks. Physical Review E. 2004; 69:026113.

Onnela JP, Saramaki J, Kertesz J, Kaski K. Intensity and coherence of motifs in weighted complex networks. Physical Review E. 2005; 71:065103.

Opitz A, Fox MD, Craddock RC, Colcombe S, Milham MP. An Integrated Framework For Targeting Functional Networks via Transcranial Magnetic Stimulation. NeuroImage. 2016; 127:86–96. [PubMed: 26608241]

Patel R, Spreng RN, Shin LM, Girard TA. Neurocircuitry models of posttraumatic stress disorder and beyond: a meta-analysis of functional neuroimaging studies. Neurosci Biobehav Rev. 2012; 36:2130–2142. [PubMed: 22766141]

Power JD, Barnes KA, Snyder AZ, Schlaggar BL, Petersen SE. Spurious but systematic correlations in functional connectivity MRI networks arise from subject motion. NeuroImage. 2012; 59:2142–2154. [PubMed: 22019881]

Power JD, Cohen AL, Nelson SM, Wig GS, Barnes KA, Church JA, Vogel AC, Laumann TO, Miezin FM, Schlaggar BL, Petersen SE. Functional network organization of the human brain. Neuron. 2011; 72:665–678. [PubMed: 22099467]

Power JD, Mitra A, Laumann TO, Snyder AZ, Schlaggar BL, Petersen SE. Methods to detect, characterize, and remove motion artifact in resting state fMRI. NeuroImage. 2014; 84:320–341. [PubMed: 23994314]

Qin LD, Wang Z, Sun YW, Wan JQ, Su SS, Zhou Y, Xu JR. A preliminary study of alterations in default network connectivity in post-traumatic stress disorder patients following recent trauma. Brain Res. 2012; 1484:50–56. [PubMed: 23010311]

Reuveni I, Bonne O, Giesser R, Shragai T, Lazarovits G, Isserles M, Schreiber S, Bick AS, Levin N. Anatomical and functional connectivity in the default mode network of post-traumatic stress disorder patients after civilian and military-related trauma. Hum Brain Mapp. 2016; 37:589–599. [PubMed: 26536845]

Ross DA, Arbuckle MR, Travis MJ, Dwyer JB, van Schalkwyk GI, Ressler KJ. An Integrated Neuroscience Perspective on Formulation and Treatment Planning for Posttraumatic Stress Disorder: An Educational Review. JAMA Psychiatry. 2017; 74:407–415. [PubMed: 28273291]

Rubinov M, Sporns O. Complex network measures of brain connectivity: uses and interpretations. NeuroImage. 2010; 52:1059–1069. [PubMed: 19819337]

Rubinov M, Sporns O. Weight-conserving characterization of complex functional brain networks. NeuroImage. 2011; 56:2068–2079. [PubMed: 21459148]

Sheynin J, Liberzon I. Circuit dysregulation and circuit-based treatments in posttraumatic stress disorder. Neurosci Lett. 2016

Shin LM, Lasko NB, Macklin ML, Karpf RD, Milad MR, Orr SP, Goetz JM, Fischman AJ, Rauch SL, Pitman RK. Resting metabolic activity in the cingulate cortex and vulnerability to posttraumatic stress disorder. Arch Gen Psychiatry. 2009; 66:1099–1107. [PubMed: 19805700]

Sporns O, Betzel RF. Modular Brain Networks. Annual review of psychology. 2016; 67:613–640.

Sripada RK, King AP, Welsh RC, Garfinkel SN, Wang X, Sripada CS, Liberzon I. Neural dysregulation in posttraumatic stress disorder: evidence for disrupted equilibrium between salience and default mode brain networks. Psychosom Med. 2012; 74:904–911. [PubMed: 23115342]

Suo X, Lei D, Li K, Chen F, Li F, Li L, Huang X, Lui S, Li L, Kemp GJ, Gong Q. Disrupted brain network topology in pediatric posttraumatic stress disorder: A resting-state fMRI study. Hum Brain Mapp. 2015; 36:3677–3686. [PubMed: 26096541]

Traud AL, Kelsic ED, Mucha PJ, Porter MA. Comparing Community Structure to Characteristics in Online Collegiate Social Networks. SIAM Review. 2011; 53:526–543.

Tursich M, Ros T, Frewen PA, Kluetsch RC, Calhoun VD, Lanius RA. Distinct intrinsic network connectivity patterns of post-traumatic stress disorder symptom clusters. Acta Psychiatr Scand. 2015; 132:29–38. [PubMed: 25572430]

van den Heuvel MP, de Lange SC, Zalesky A, Seguin C, Yeo BTT, Schmidt R. Proportional thresholding in resting-state fMRI functional connectivity networks and consequences for patient-control connectome studies: Issues and recommendations. NeuroImage. 2017; 152:437–449. [PubMed: 28167349]

van Wijk BC, Stam CJ, Daffertshofer A. Comparing brain networks of different size and connectivity density using graph theory. PLoS One. 2010; 5:e13701. [PubMed: 21060892]

Watts DJ, Strogatz SH. Collective dynamics of ‘small-world’ networks. Nature. 1998; 393:440–442. [PubMed: 9623998]

Whitfield-Gabrieli S, Bauer C, Okano K, Nestor P, Del Re E, Gosh S, Niznikiewicz M. M64. Real Time fMRI Feedback Targeting Default Mode Network (DMN) Reduces Auditory Hallucinations. Schizophrenia Bulletin. 2017; 43:S233–S233.

Wu RZ, Zhang JR, Qiu CJ, Meng YJ, Zhu HR, Gong QY, Huang XQ, Zhang W. Study on resting-state default mode network in patients with posttraumatic stress disorder after the earthquake. Sichuan Da Xue Xue Bao Yi Xue Ban. 2011; 42:397–400. [PubMed: 21827007]

Xia M, Wang J, He Y. BrainNet Viewer: a network visualization tool for human brain connectomics. PLoS One. 2013; 8:e68910. [PubMed: 23861951]

Yamasue H, Kasai K, Iwanami A, Ohtani T, Yamada H, Abe O, Kuroki N, Fukuda R, Tochigi M, Furukawa S. Voxel-based analysis of MRI reveals anterior cingulate gray-matter volume reduction in posttraumatic stress disorder due to terrorism. Proceedings of the National Academy of Sciences. 2003; 100:9039–9043.

Yang J, Leskovec J. Defining and evaluating network communities based on ground-truth. Knowledge and Information Systems. 2015; 42:181–213.

Yendiki A, Koldewyn K, Kakunoori S, Kanwisher N, Fischl B. Spurious group differences due to head motion in a diffusion MRI study. NeuroImage. 2014; 88:79–90. [PubMed: 24269273]

Yendiki A, Panneck P, Srinivasan P, Stevens A, Zollei L, Augustinack J, Wang R, Salat D, Ehrlich S, Behrens T, Jbabdi S, Gollub R, Fischl B. Automated probabilistic reconstruction of white-matter pathways in health and disease using an atlas of the underlying anatomy. Front Neuroinform. 2011; 5:23. [PubMed: 22016733]

Yeo BT, Krienen FM, Sepulcre J, Sabuncu MR, Lashkari D, Hollinshead M, Roffman JL, Smoller JW, Zollei L, Polimeni JR, Fischl B, Liu H, Buckner RL. The organization of the human cerebral cortex estimated by intrinsic functional connectivity. J Neurophysiol. 2011; 106:1125–1165. [PubMed: 21653723]

Zalesky A, Fornito A, Bullmore E. On the use of correlation as a measure of network connectivity. NeuroImage. 2012; 60:2096–2106. [PubMed: 22343126]

Zalesky A, Fornito A, Bullmore ET. Network-based statistic: identifying differences in brain networks. NeuroImage. 2010; 53:1197–1207. [PubMed: 20600983]

Zalesky A, Fornito A, Cocchi L, Gollo LL, van den Heuvel MP, Breakspear M. Connectome sensitivity or specificity: which is more important? NeuroImage. 2016; 142:407–420. [PubMed: 27364472]

Zhou Y, Wang Z, Qin LD, Wan JQ, Sun YW, Su SS, Ding WN, Xu JR. Early altered resting-state functional connectivity predicts the severity of post-traumatic stress disorder symptoms in acutely traumatized subjects. PLoS One. 2012; 7:e46833. [PubMed: 23056477]

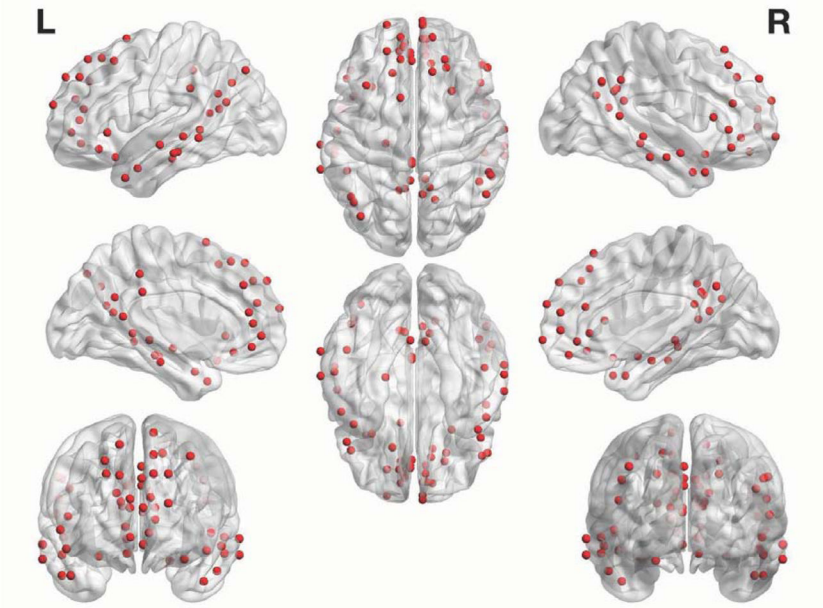

Figure 1. DMN Nodes

Figure depicts the 64 nodes from the functional atlas comprising the DMN that we used for the primary analysis.

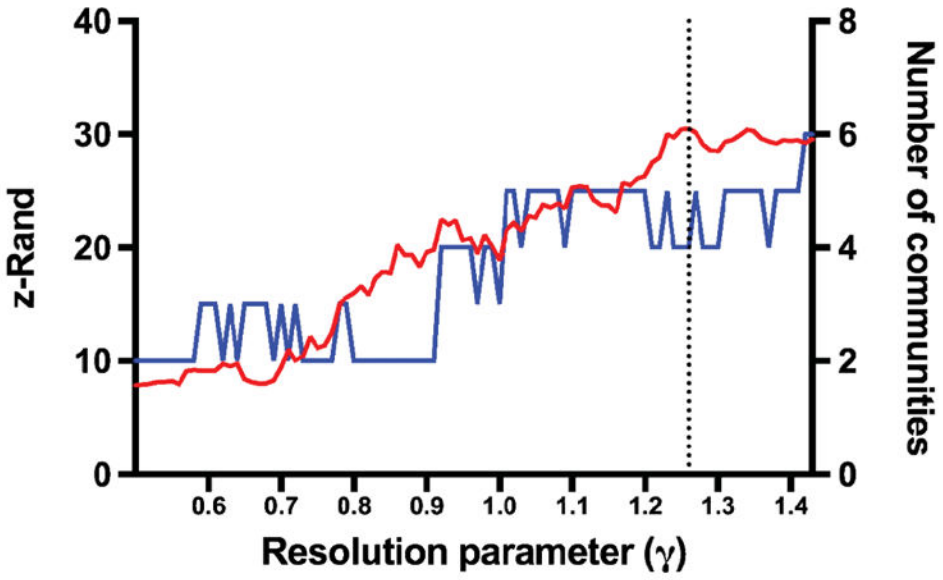

Figure 2. Identification of candidate resolution parameters

Plot representing the z-Rand scores and number of communities for each resolution parameter (γ). The number of communities were determined after the association-reclustering step. The dashed line represents the local z-Rand maximum (30.5), corresponding to $\gamma = 1.26$, at which the outputs of the Louvain algorithm were most stable (while the total number of communities remained ≤ 6).

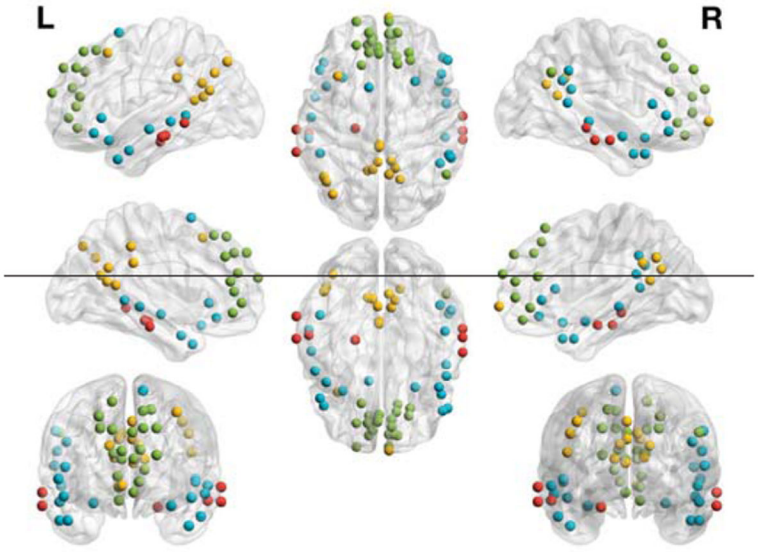

Figure 3. The partition solution resulting in 4 DMN communities

A predominantly posterior community (yellow; PCC, precuneus, and left angular gyrus), a frontal community (green; vmPFC and dmPFC), an MT-parahippocampal (MT-P community (red; middle temporal and parahippocampal cortex), and an MT-inferior frontal (MT-IF) community (blue).

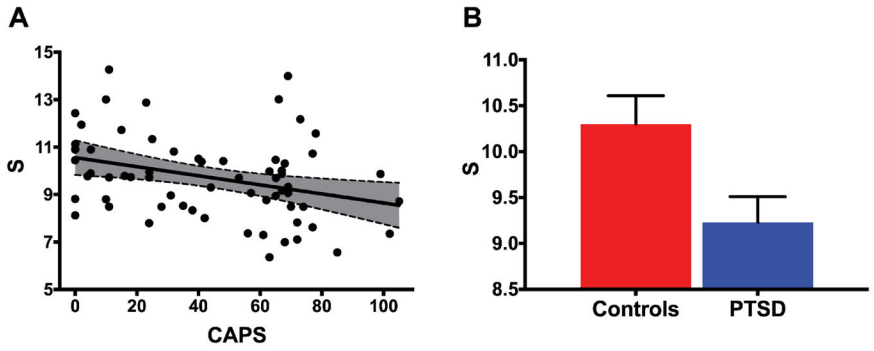

Figure 4. PTSD and DMN connectivity strength

(A) Scatter plot depicting the correlation between PTSD severity, as measured by the Clinician Administered PTSD Scale (CAPS), and DMN overall connectivity strength (*S*) [$r_{(64)} = -0.329$, $p = 0.0075$]. The gray area is the 95% confidence band of the best-fit line. (B) Bar graph depicting means and standard error of *S* across groups [CC: mean = 10.30 ± 0.31; PTSD: mean = 9.23 ± 0.28; $p = 0.014$].

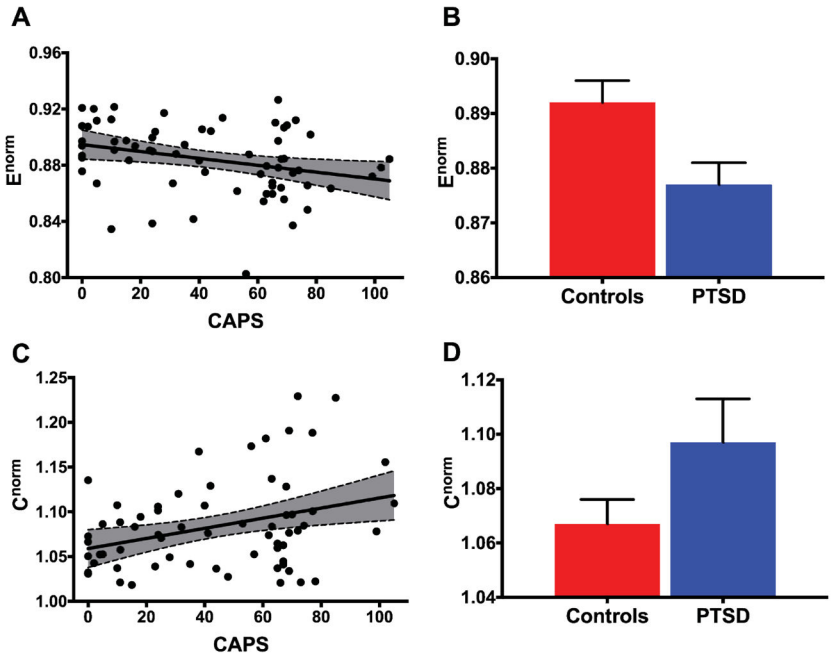

Figure 5. PTSD and DMN integration and segregation

(A–B) Scatter plots depicting the correlation between PTSD severity, as measured by the Clinician Administered PTSD Scale (CAPS), and DMN integration and segregation. The gray area is the 95% confidence band of the best-fit line. (A) represents the normalized global efficiency [E^{norm}: $r_{(64)} = -0.299$, $p = 0.0157$]; (B) represents the clustering coefficient [C^{norm}: $r_{(64)} = 0.334$, $p = 0.0065$]. (C–D) Bar graphs depicting means and standard error of E^{norm}: [CC: mean = 0.892 ± 0.004; PTSD: mean = 0.877 ± 0.004; $p = 0.01$], and C^{norm}: [CC: mean = 1.067 ± 0.009; PTSD: mean = 1.097 ± 0.008; $p = 0.016$], across the CC and PTSD groups.

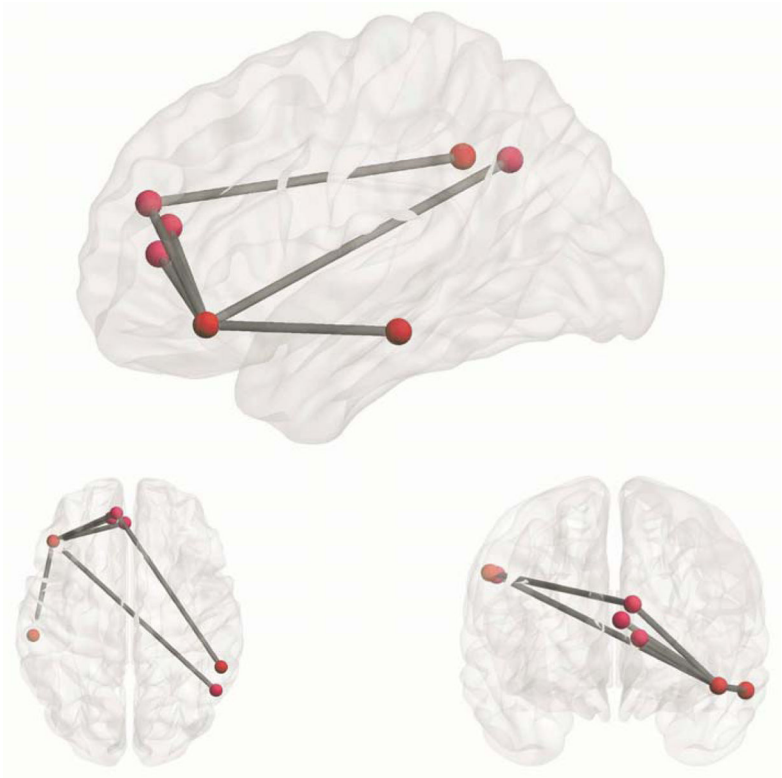

Figure 6. Sub-network within the DMN negatively associated with PTSD severity after correcting for family-wise error

Connections represent edges that were negatively associated with CAPS severity after correction for multiple comparisons with NBS. Note that all abnormal edges involve the PFC (mPFC and lateral orbitofrontal cortex).